Oxygen Reduction

DOI: 10.1002/anie.201104004

$Co_{1-x}S$–Graphene Hybrid: A High-Performance Metal Chalcogenide Electrocatalyst for Oxygen Reduction**

*Hailiang Wang, Yongye Liang, Yanguang Li, and Hongjie Dai**

Owing to their high energy-conversion efficiency, low or even zero emission, and high energy and power density, fuel cells such as proton-exchange membrane fuel cells (PEMFC) and direct methanol fuel cells (DMFC) have drawn tremendous attention as potential clean and efficient power sources for both electric vehicles and portable electronics.[1,2] A major limiting factor of energy-conversion efficiency for present fuel cells is the sluggish kinetics of the oxygen reduction reaction (ORR) at the cathode.[3–9] Platinum and its alloys have been so far the most active ORR catalysts.[3–9] However, the prohibitive cost, scarcity, and declining activity of Pt-based catalysts have hindered widespread application and commercialization of fuel cells.[3–9] Consequently, alternative electrocatalysts based on nonprecious metals have been actively pursued.[3–9]

Cobalt sulfides have been investigated as ORR catalyst with the highest activity among all chalcogenides of nonprecious metals in acidic solution.[2,10–16] Theoretical studies predicted electrocatalytic activity of Co_9S_8 similar to that of Pt via a four-electron ORR pathway.[11] However, current ORR catalysts based on cobalt sulfides and cobalt selenides have exhibited activities far lower than that of Pt.[12–16] Moreover, it has been shown that two-electron reduction is the dominant reaction pathway for cobalt sulfide catalysts, especially at potentials higher than 0.5 V versus the reversible hydrogen electrode (RHE).[2] It is thus highly desirable to design and synthesize high-performance cobalt chalcogenide based electrocatalyst materials capable of catalyzing four-electron ORR.

Here we describe a novel cobalt sulfide–graphene hybrid electrocatalyst for ORR, obtained by controlled two-step synthesis of $Co_{1-x}S$ nanoparticles on reduced graphene oxide (RGO). The RGO sheets underlying the $Co_{1-x}S$ nanoparticles provide an electrically conducting support for the catalyst, control the size of the catalyst particles, and enhance the ORR catalytic activity of the $Co_{1-x}S$ nanoparticles through strong electrochemical coupling. In 0.5 M H_2SO_4, our $Co_{1-x}S$/RGO hybrid catalyst shows an ORR current onset at about 0.8 V versus RHE. When the electrode is rotated at 1600 rpm, the ORR current density is as high as about 1.1 mA cm^{-2} at 0.7 V versus RHE with a loading of about 100 μg cm^{-2}. Measurements with both rotating disk electrode (RDE) and rotating ring disk electrode (RRDE) show that nearly four-electron ORR can be achieved with the $Co_{1-x}S$/RGO hybrid catalyst. The $Co_{1-x}S$/RGO hybrid is the highest performance ORR catalyst among all cobalt chalcogenide based materials reported in the literature.

Cobalt sulfide nanoparticles were synthesized on RGO sheets by a low-temperature solution-phase reaction followed by a high-temperature annealing step. Graphene oxide (GO) was made by a modified Hummers method (see Supporting Information), in which a six times lower concentration of $KMnO_4$ was used (see Supporting Information) to give GO sheets with lower oxygen content than Hummers GO (ca. 15 vs. ca. 30%, measured by X-ray photoelectron spectroscopy (XPS) and Auger spectroscopy).[17–19] In the first reaction step, nanoparticles of cobalt sulfide precursor were selectively and uniformly coated onto GO surface by treating $Co(OAc)_2$ with thioacetamide (TAA) in a GO/water suspension at 80 °C for 12 h (Figure S1, Supporting Information). The intermediate product was then annealed at 500 °C in 1 atm of Ar for 1 h to give the final hybrid material of cobalt sulfide nanoparticles on graphene (see Supporting Information for experimental details). Scanning electron microscopy (SEM) and transmission electron microscopy (TEM) clearly revealed that cobalt sulfide nanoparticles were selectively grown on RGO sheets without free growth of unattached nanoparticles in solution (Figure 1a, b, and d). The cobalt sulfide nanoparticles on RGO were crystalline with an average particle size of about 10–20 nm (Figure 1b and d). X-ray diffraction (XRD, Figure 1c) showed that the cobalt sulfide nanoparticles grown on RGO are a $Co_{1-x}S$ phase (ICDD PDF #00-042-0826) with hexagonal structure in space group $P6_3/mmc$ (no. 194). The lattice fringes of the $Co_{1-x}S$ nanocrystals (Figure 1d) and the electron diffraction pattern (Figure 1d inset) are consistent with the crystal structure. The $Co_{1-x}S$/RGO hybrid contains about 30 wt% of RGO with a designed Co/C ratio of 1/4.

The ORR catalytic activity of $Co_{1-x}S$/RGO was first characterized by loading the hybrid material onto glassy carbon electrode for cyclic voltammetry (CV) measurements in 0.5 M H_2SO_4 at 25 °C (see Supporting Information for experimental details). Comparison of CV curves in O_2- versus Ar-saturated electrolyte clearly revealed the ORR catalytic activity of $Co_{1-x}S$/RGO. The hybrid showed an ORR onset potential at about 0.8 V versus RHE, and the peak current was reached at about 0.73 V versus RHE (Figure 2a).

Measurements with an RDE were carried out to reveal the ORR kinetics of the $Co_{1-x}S$/RGO hybrid in 0.5 M H_2SO_4 (Figure 2b). At 1600 rpm, the $Co_{1-x}S$/RGO hybrid catalyst showed a current density of about 1.1 mA cm^{-2} at 0.7 V versus

[*] H. Wang, Y. Liang, Y. Li, Prof. H. Dai
Department of Chemistry, Stanford University, Keck Building
380 Roth Way, Stanford, CA 94305 (USA)
E-mail: hdai@stanford.edu

[**] This work is supported partially by ONR and a Stanford Graduate Fellowship.

Supporting information for this article is available on the WWW under http://dx.doi.org/10.1002/anie.201104004.

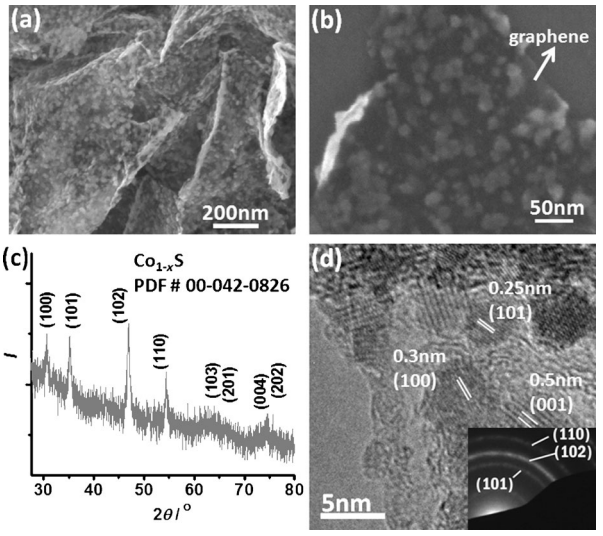

Figure 1. a) Low-magnification SEM image of $Co_{1-x}S$/RGO deposited on a silicon substrate from a suspension in solution. b) High-magnification SEM image of $Co_{1-x}S$ nanoparticles grown on RGO. c) XRD spectrum of a compacted film of $Co_{1-x}S$/RGO. d) TEM image of $Co_{1-x}S$/RGO hybrid with an inset electron diffraction pattern of $Co_{1-x}S$ nanocrystals grown on RGO.

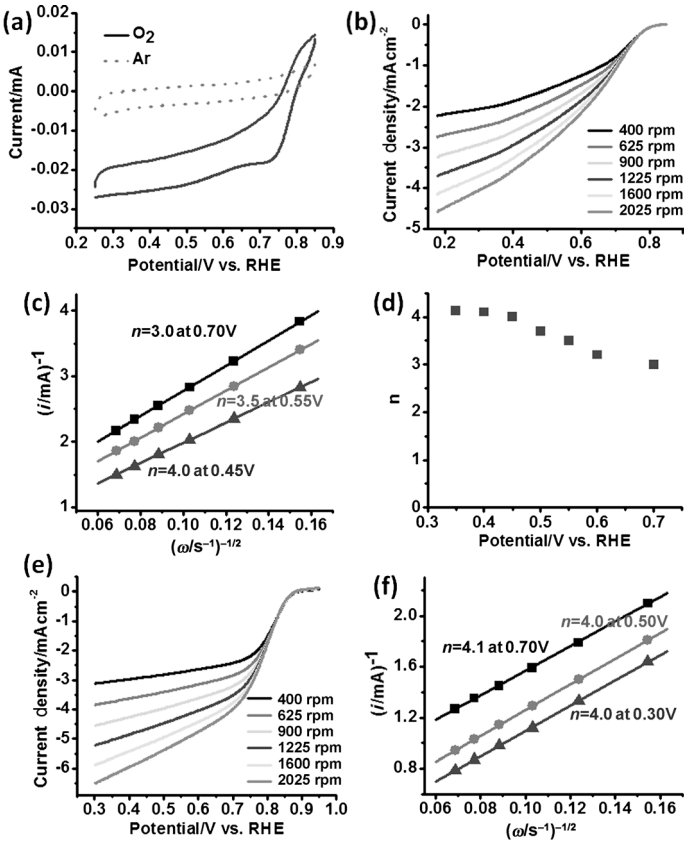

Figure 2. a) CV curves of $Co_{1-x}S$/RGO hybrid on glassy carbon electrodes in O_2-saturated (solid line) and Ar-saturated (dotted line) 0.5 M H_2SO_4 with a sweep rate of 10 mV s^{-1}. Catalyst loading was 0.285 mg cm^{-2}. b) RDE curves of $Co_{1-x}S$/RGO (loading ca. 0.1 mg cm^{-2}) in O_2-saturated 0.5 M H_2SO_4 with a sweep rate of 5 mV s^{-1} at different rotation rates. c) Corresponding Koutecky–Levich plots (i^{-1} vs. $\omega^{-0.5}$) at different potentials for RDE curves in b). d) Electron-transfer number n derived from Koutecky–Levich plots at different potentials. e) RDE curves of $Co_{1-x}S$/RGO (loading ca. 0.1 mg cm^{-2}) in O_2-saturated 0.1 M KOH with a sweep rate of 5 mV s^{-1} at different rotation rates. f) Corresponding Koutecky–Levich plots (i^{-1} vs. $\omega^{-0.5}$) at different potentials for RDE curves in (e).

RHE, higher than that of any other cobalt chalcogenide catalysts, including a recently reported $CoSe_2$/Pt composite, at identical potentials also in 0.5 M H_2SO_4.[12–16] The hybrid reached a current density of about 4.2 mA cm^{-2} at 0.18 V versus RHE, which is close to the diffusion-limited current density expected for four-electron transfer in 0.5 M H_2SO_4.[2] The electron-transfer number n was derived from the slopes of Koutecky–Levich plots at various potentials (Figure 2c and Supporting Information).[2,20,21] At low overpotential (0.7 V vs. RHE), $n \approx 3.0$ was calculated, indicating both two- and four-electron reductions taking place (Figure 2c and d). When the potential was polarized in the more negative direction, n increased to approach 4.0 at 0.45 V versus RHE (Figure 2c and d). At potentials lower than 0.45 V versus RHE, n remained close to 4, suggesting nearly four-electron reduction of O_2 in this potential region (Figure 2d). RDE measurements were also carried out in 0.5 M H_2SO_4 for the $Co_{1-x}S$/RGO hybrid (ca. 30 wt% RGO) with various loadings (Figure S2a, Supporting Information) and another two $Co_{1-x}S$/RGO hybrids (ca. 20 and ca. 50 wt% of RGO, respectively) with different Co/C ratios (Figure S2b, Supporting Information). Similar ORR performance was obtained in an approximate Co/C atomic ratio range of 1/8 to 1/2 (Figure S2b, Supporting Information).

The $Co_{1-x}S$/RGO hybrid also showed high ORR catalytic activity in basic solution. RDE measurements on the hybrid catalyst were carried out in 0.1 M KOH solution (Figure 2e). At 1600 rpm, the hybrid catalyst showed an ORR onset potential of about 0.87 V versus RHE. The ORR current density at 1600 rpm was about 3.8 mA cm^{-2} at 0.7 V versus RHE, and reached about 5.8 mA cm^{-2} (diffusion-limited current for four-electron transfer in 0.1 M KOH) at 0.3 V versus RHE. The n value was calculated to be approximately 4 throughout the potential range studied (Figure 2f).

Measurements with an RRDE were also carried out to investigate the two-electron versus the four-electron reduction pathway and the percentage of hydrogen peroxide production in ORR catalyzed by the $Co_{1-x}S$/RGO hybrid material in 0.5 M H_2SO_4. At 1600 rpm, the ring current (H_2O_2 oxidation) was much smaller than the disk current (oxygen reduction), that is, H_2O was the main product of ORR catalyzed by the hybrid (Figure 3a). The percentage of two-electron oxygen reduction calculated from RRDE curves in Figure 3a is shown in Figure 3b. The two-electron pathway accounted for 30% of the ORR at low overpotential (0.7 V vs. RHE), which corresponds to $n \approx 3.4$ (Figure 3c). When the potential was polarized more towards the negative, the percentage of two-electron reduction steadily decreased to about 10% with $n \approx 3.8$ at 0.18 V versus RHE, that is, nearly four-electron reduction. RRDE measurements were also carried out for $Co_{1-x}S$/RGO hybrids with various loadings (Figure S3, Supporting Information). More H_2O_2 was produced at 0.05 mg cm^{-2} than at 0.1 mg cm^{-2} and 0.2 mg cm^{-2}

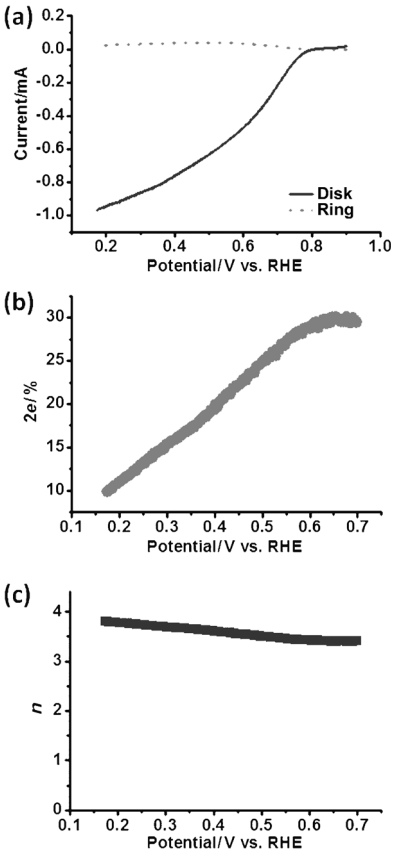

Figure 3. a) RRDE curves of $Co_{1-x}S$/RGO (loading ca. 0.1 mg cm^{-2}) in O_2-saturated 0.5 M H_2SO_4 with a sweep rate of 5 mV s^{-1} at a rotation rate of 1600 rpm. b) Percentage of two-electron reduction in ORR at different potentials calculated from RRDE curves in (a). c) Electron-transfer number *n* at different potentials calculated from RRDE curves in a)

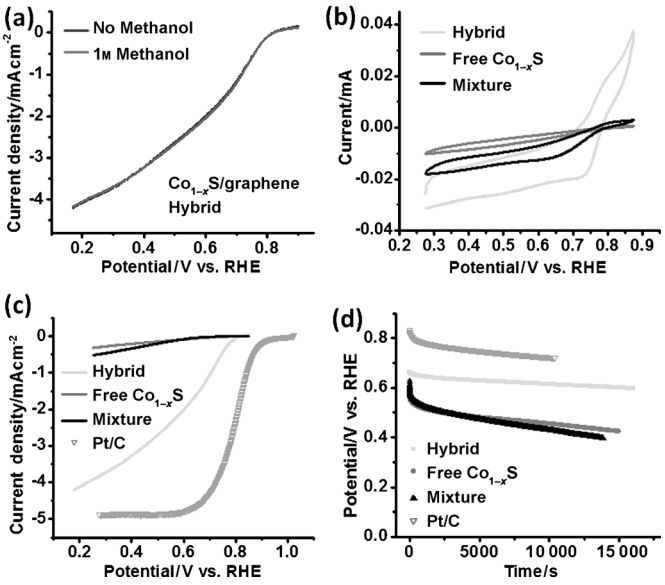

Figure 4. a) RDE curves of $Co_{1-x}S$/RGO hybrid at a rotation rate of 1600 rpm in O_2-saturated 0.5 M H_2SO_4 with and without 1 M of methanol. Sweep rate was 5 mV s^{-1}. Catalyst loading was 0.1 mg cm^{-2}. b) CV curves of $Co_{1-x}S$/RGO hybrid, free $Co_{1-x}S$ nanoparticles, and physical mixture of RGO and $Co_{1-x}S$ nanoparticles on glassy carbon electrodes in O_2-saturated 0.5 M H_2SO_4 with a sweep rate of 10 mV s^{-1}. Catalyst loading was 0.285 mg cm^{-2} for all samples. c) RDE curves of $Co_{1-x}S$/RGO hybrid, free $Co_{1-x}S$ nanoparticles, physical mixture of RGO and $Co_{1-x}S$ nanoparticles, and Pt/C at a rotation rate of 1600 rpm in O_2-saturated 0.5 M H_2SO_4 with a sweep rate of 5 mV s^{-1}. Catalyst loading was 0.1 mg cm^{-2} for all samples. d) Galvanostatic constant-current discharge curves of $Co_{1-x}S$/RGO hybrid, free $Co_{1-x}S$ nanoparticles, physical mixture of RGO and $Co_{1-x}S$ nanoparticles, and Pt/C at a rotation rate of 1600 rpm in O_2-saturated 0.5 M H_2SO_4. Discharge current density was about 1.5 mA cm^{-2} for $Co_{1-x}S$/RGO hybrid, about 0.05 mA cm^{-2} for free $Co_{1-x}S$ nanoparticles and physical mixture of RGO and $Co_{1-x}S$ nanoparticles, and about 1.5 mA cm^{-2} for Pt/C.

(Figure S3, Supporting Information), similar to the cases of $CoSe_2$ and Pt in the literature.[15,22]

A commercial Pt/C catalyst (Etek) showed about 0.1–0.15 V lower ORR overpotential than $Co_{1-x}S$/RGO in 0.5 M H_2SO_4 (Figure S4a, Supporting Information). However, the ORR catalytic activity of Pt/C was significantly decreased by adding methanol to the electrolyte (Figure S4b, Supporting Information). In contrast, the $Co_{1-x}S$/RGO hybrid catalyst was not affected by methanol (Figure 4a), and this makes it a promising inexpensive cathode electrocatalyst for DMFC.

Various cobalt sulfide and cobalt selenide ORR catalysts have been prepared by different methods, such as solvothermal reactions, sputtering, and surfactant-free solution-phase reactions.[12–16] With similar mass loadings, the $Co_{1-x}S$/RGO hybrid catalyst can deliver higher ORR current density than any other reported cobalt chalcogenide based catalysts at equal potentials in acidic media.[12–16] The high ORR catalytic performance of $Co_{1-x}S$/RGO is attributed to the intimate coupling between the $Co_{1-x}S$ nanoparticles and RGO, due to the direct nucleation and growth approach. The $Co_{1-x}S$ nanoparticles are electrically wired to the RGO sheets, which form a conducting network to the electrode and facilitate ORR through facile charge transport between oxygen molecules adsorbed on $Co_{1-x}S$ active sites and the electrode. Growth of nanoparticles on RGO also afforded much more desirable morphology and smaller sizes of the $Co_{1-x}S$ nanoparticles due to RGO serving as a substrate with oxygen functional groups for nucleation of nanomaterials. The interactions between functional groups on RGO and $Co_{1-x}S$ nanoparticles during nucleation and growth lead to small catalyst particles and thus enhanced surface area and active catalytic sites in the hybrid material, which contribute to higher ORR current density. Without graphene oxide in the growth solution, only large secondary particles were produced by the same synthetic procedures (Figure S5, Supporting Information).

Both free $Co_{1-x}S$ particles grown in solution without graphene and their physical mixture with RGO showed inferior ORR catalytic activity to the $Co_{1-x}S$/RGO hybrid in 0.5 M H_2SO_4 (Figure 4a and b). Moreover, $Co_{1-x}S$/RGO also showed reasonable ORR catalytic stability in 0.5 M H_2SO_4, much higher than that of the free $Co_{1-x}S$ particles and their mixture with RGO, as measured by constant-current galvanostatic discharge (Figure 4c). With the $Co_{1-x}S$/RGO hybrid catalyst, the potential decreased from about 0.65 to about 0.60 V in 15000 s at a constant discharge current density of

about 1.5 mA cm^{-2} and a catalyst loading of about 0.1 mg cm^{-2}. Reasonable stability of the $Co_{1-x}S$/RGO hybrid catalyst was also observed in CV measurements in 0.5 M H_2SO_4, in which the ORR current decreased only slightly after 10000 cycles (Figure S6, Supporting Information).

Further analysis of the electrochemical data of $Co_{1-x}S$/RGO hybrid, free $Co_{1-x}S$, and mixture of $Co_{1-x}S$ and RGO supports the mechanism proposed for $Co_{1-x}S$/RGO above. We observed that free $Co_{1-x}S$ and its mixture with RGO showed similar ORR onset potential to the hybrid catalyst (Figure 4b and c), although the ORR current densities were much lower. This strongly suggests that the ORR active sites of the three catalysts above originate from $Co_{1-x}S$. Mixing with RGO and growth on RGO both make the $Co_{1-x}S$ more conducting and increase the ORR current density, whereby the latter is much more effective than the former. Furthermore, growth on RGO reduces the size and increases the surface area of the $Co_{1-x}S$ nanoparticles, which could also contribute to the high ORR current density. In impedance spectroscopy measurements, the $Co_{1-x}S$/RGO hybrid showed a much smaller semicircle than the corresponding mixture in the potential region where ORR is taking place (Figure S7, Supporting Information), which indicates much smaller charge-transfer resistance due to nanoparticle–graphene electron transport or much faster mass diffusion due to the hybrid structure of nanoparticles grown on graphene.[23,24]

Interestingly, a CoS_2/RGO hybrid material was also obtained by 180 °C hydrothermal treatment (instead of the annealing step) of the product derived from the first step of reaction at 80 °C. We found CoS_2 (cubic structure, space group $Pa\bar{3}$ (no. 205), ICDD PDF #00-041-1471) nanoparticles selectively grown on RGO with an average size of about 50 nm, larger than that of the precursor nanoparticles from the first step of reaction, likely due to Oswald ripening and recrystallization under hydrothermal conditions (Figure S8a and S8b, Supporting Information).[25] The ORR catalytic activity of the CoS_2/RGO hybrid made hydrothermally was lower than that of the above $Co_{1-x}S$/RGO hybrid in 0.5 M H_2SO_4, likely due to the larger size of the cobalt sulfide nanoparticles and different crystal phase, but was still much higher than that of free $Co_{1-x}S$ particles without graphene or their physical mixture with RGO (Figure S8c and S8d, Supporting Information). This suggested that the second step gas-phase annealing in making the $Co_{1-x}S$/RGO hybrid is important in controlling the size, phase, and morphology of the cobalt sulfide nanoparticles grown on graphene for optimum ORR catalytic performance.

In summary, a $Co_{1-x}S$/RGO hybrid material was synthesized by a mild solution-phase reaction followed by a solid-state annealing step. Strong electrochemical coupling of the RGO support with the $Co_{1-x}S$ nanoparticles directly grown on top and the desirable morphology, size, and phase of the $Co_{1-x}S$ nanoparticles mediated by the RGO template afford unprecedented high ORR catalytic performance among all cobalt chalcogenide based ORR catalysts.

Received: June 11, 2011
Revised: August 24, 2011
Published online: September 23, 2011

Keywords: chalcogenides · cobalt · electrochemistry · nanoparticles · oxygen reduction

[1] M. Winter, R. J. Brodd, *Chem. Rev.* **2004**, *104*, 4245 – 4269.
[2] *PEM Fuel Cell Electrocatalysts and Catalyst Layers: Fundamentals and Applications* (Ed.: J. Zhang), Springer, New York, **2008**.
[3] A. A. Gewirth, M. S. Thorum, *Inorg. Chem.* **2010**, *49*, 3557 – 3566.
[4] B. Wang, *J. Power Sources* **2005**, *152*, 1 – 15.
[5] C. Zhong, J. Luo, B. Fang, B. N. Wanjala, P. N. Njoki, R. Loukrakpam, J. Yin, *Nanotechnology* **2010**, *21*, 062001.
[6] A. Morozan, B. Jousselme, S. Palacin, *Energy Environ. Sci.* **2011**, *4*, 1238 – 1254.
[7] *Fuel Cell Science: Theory, Fundamentals, and Biocatalysis* (Eds.: A. Wieckowski, J. K. Nørskov), Wiley, Hoboken, **2010**.
[8] V. Stamenkovic, B. S. Mun, K. J. J. Mayrhofer, P. N. Ross, N. M. Markovic, J. Rossmeisl, J. Greeley, J. K. Nørskov, *Angew. Chem.* **2006**, *118*, 2963 – 2967; *Angew. Chem. Int. Ed.* **2006**, *45*, 2897 – 2901.
[9] R. Srivastava, P. Mani, N. Hahn, P. Strasser, *Angew. Chem.* **2007**, *119*, 9146 – 9149; *Angew. Chem. Int. Ed.* **2007**, *46*, 8988 – 8991.
[10] N. Alonso-Vante, H. Tributsch, *Nature* **1986**, *323*, 431 – 432.
[11] R. A. Sidik, A. B. Anderson, *J. Phys. Chem. B* **2006**, *110*, 936 – 941.
[12] Y. Zhou, H. Yao, Y. Wang, H. Liu, M. Gao, P. Shen, S. Yu, *Chem. Eur. J.* **2010**, *16*, 12000 – 12007.
[13] L. Zhu, D. Susaca, M. Teoa, K. C. Wong, P. C. Wong, R. R. Parsons, D. Bizzotto, K. A. R. Mitchell, S. A. Campbell, *J. Catal.* **2008**, *258*, 235 – 242.
[14] Y. J. Feng, T. He, N. Alonso-Vante, *Chem. Mater.* **2008**, *20*, 26 – 28.
[15] Y. J. Feng, T. He, N. Alonso-Vante, *Fuel Cells* **2010**, *10*, 77 – 83.
[16] M. Gao, Q. Gao, J. Jiang, C. Cui, W. Yao, S. Yu, *Angew. Chem.* **2011**, *123*, 5007 – 5010; *Angew. Chem. Int. Ed.* **2011**, *50*, 4905 – 4908.
[17] H. Wang, L. Cui, Y. Yang, H. S. Casalongue, J. T. Robinson, Y. Liang, Y. Cui, H. Dai, *J. Am. Chem. Soc.* **2010**, *132*, 13978 – 13980.
[18] Y. Li, H. Wang, L. Xie, Y. Liang, G. Hong, H. Dai, *J. Am. Chem. Soc.* **2011**, *133*, 7296 – 7299.
[19] Y. Liang, Y. Li, H. Wang, J. Zhou, J. Wang, T. Regier, H. Dai, *Nat. Mater.*, DOI: 10.1038/nmat3087.
[20] K. J. J. Mayrhofer, D. Strmcnik, B. B. Blizanac, V. Stamenkovic, M. Arenz, N. M. Markovic, *Electrochim. Acta* **2008**, *53*, 3181 – 3188.
[21] *Electrochemical Methods: Fundamentals and Aplications* (Eds.: A. J. Bard, L. R. Faulkner), Wiley, New York, **2001**.
[22] N. Alonso-Vante, *ChemPhysChem* **2010**, *11*, 2732 – 2744.
[23] L. Genies, Y. Bultel, R. Faure, R. Durand, *Electrochim. Acta* **2003**, *48*, 3879 – 3890.
[24] Q. He, X. Yang, W. Chen, S. Mukerjee, B. Koel, S. Chen, *Phys. Chem. Chem. Phys.* **2010**, *12*, 12544 – 12555.
[25] H. Wang, J. T. Robinson, G. Diankov, H. Dai, *J. Am. Chem. Soc.* **2010**, *132*, 3270 – 3271.

